Coordination Chemistry Reviews 257 (2013) 2737–2751

Contents lists available at ScienceDirect

Coordination Chemistry Reviews

journal homepage: www.elsevier.com/locate/ccr

Review

Nickel binding sites in histone proteins: Spectroscopic and structural characterization

Massimiliano Peana[a,*], Serenella Medici[a,1], Valeria Marina Nurchi[b], Guido Crisponi[b], Maria Antonietta Zoroddu[a,*]

[a] Department of Chemistry and Pharmacy, University of Sassari, Sassari, Italy
[b] Department of Chemical and Geological Sciences, University of Cagliari, Cittadella Universitaria, I-09042 Monserrato, Italy

Contents

ARTICLE INFO

Article history:
Received 30 November 2012
Received in revised form 13 February 2013
Accepted 19 February 2013
Available online 7 March 2013

Keywords:
Ni(II) ions
Histone proteins
Peptide fragments
Carcinogenesis

ABSTRACT

Nickel compounds are included among human carcinogens, though the molecular events related to them are not yet completely known.

It has been proposed that the basic element, in the mechanism of carcinogenesis exerted by nickel, is connected to its binding within the cell nucleus. DNA can weakly bind Ni(II), thus the nuclear proteins, in particular histones proteins which are abundantly present, could be important targets for Ni(II) ions.

The present review describes the interactions of nickel with histone H4, core tetramer $(H3\text{-}H4)_2$ and several peptide fragments which have been selected as possible candidates for specific binding sites in the histone octamer.

The collected results allowed us to propose several mechanisms for nickel-induced damage triggering from metal coordination, including structural changes of histone proteins, as well as nucleobase oxidation and sequence-specific histone hydrolysis.

1. Introduction

Nickel compounds are included among human carcinogens [1]. The responsible molecular mechanisms remain, however, still uncertain and to be fully understood.

Actually, promutagenic DNA damage and epigenetic effects in chromatin, that result from nickel binding inside the cell nucleus, are believed to be the main causes of nickel carcinogenesis [2–4]. Since there are no high affinity binding sites for Ni(II) in DNA as well as in phospholipids of cellular membranes, the proteins in the cell nucleus remain as the possible Ni(II) targets. Among the proteins inside the cell nucleus, histones are abundantly present; in fact, they can reach a concentration of around 3 mM in somatic cells [5]. Their high concentration, despite their moderate content of Ni(II) binding sites, allows them to positively compete, according to the mass action law, with less abundantly present nuclear proteins containing higher affinity binding sites or with small ligand molecules as, for example, histidine or glutathione.

* Corresponding authors. Tel.: +39 079 229529.
E-mail address: zoroddu@uniss.it (M.A. Zoroddu).
[1] Tel.: +39 079 229529.

0010-8545/$ – see front matter © 2013 Elsevier B.V. All rights reserved.
http://dx.doi.org/10.1016/j.ccr.2013.02.022

Several authors have given evidence of such sites on core histones [6,7]. According them, nucleohistones enhance to a great extent the formation of 8-oxo-7,8-dihydroxo-2′-deoxyguanosine, representing the main product of the attack of the reactive oxygen species (ROS) in genomic DNA. Moreover, exposure of chromatin to ambient oxygen in the presence of free, non complexed Ni(II) ions, different from pure DNA, increases DNA oxidation. Actually, Ni(II) species, mainly in the form of complexes with some endogenous ligands, lead to an increase of oxidation damage to nucleobases.

For these reasons, the recognition of binding sites in histones, specific for Ni(II), and their structural characterization would afford a structural-function view for a better knowledge of the mechanism by which Ni(II) induces carcinogenicity.

Ni(II), classified as a borderline metal ion, forms stable coordination compounds both with hard donor atoms, like oxygen, and with borderline and soft donor atoms, like nitrogen and sulfur. Literature data on the binding of Ni(II) to proteins and to peptides point to imidazole nitrogen of histidine and thiol of cysteine as the thermodynamically favored donor ligands for Ni(II) [8,9]; oxygen from carboxyl groups of glutamic and aspartic acids exerts a less important role in the coordination.

Mainly, two general mechanisms relative to the coordination of transition metal ions with proteins and peptides are known: the peptide mode and the protein mode. The first one involves the binding to the N-terminal amino group together with, in order to complete the chelate ring, the involvement of the nearest carbonyl oxygen acting as the second donor. The deprotonation of further peptide nitrogen atoms by metal ions occurs, by increasing the pH, until N^- amide bonds on the peptide backbone form [10]. Such a mechanism takes place in the peptides which do not bear coordinating side chains in the amino terminal residues. The protein mode instead employs coordinating side-chain groups. In particular, imidazole nitrogen of histidine and thiol of cysteine make easier peptide deprotonation, by behaving like the anchoring binding sites for metal ions. Attention should be devoted to search for histidine and cysteine residues, other than terminal sequences, as potential nickel-binding sites on histones. These groups are the most effective in Ni(II) coordination.

Here we summarize the results obtained on the structural and thermodynamic features of nickel binding sites in histones. In particular, the spectroscopic and potentiometric analysis of the metal species with model peptides have given useful information such as binding constants, chemical speciation and structural characterization of metal complexes, providing an interesting molecular view of bioinorganic chemistry of nickel induced carcinogenesis.

2. Histone proteins

H2A, H2B, H3 and H4 are the core histone proteins; they, together with H1, the linker histone, package DNA into repeating nucleosomal units folded into the fibers of chromatin.

The structure of nuclear histones is formed from globular C-terminal and random-coil N-terminal domains. The sites of post-translational modifications, such as acetylation, are located on the N-terminal tails.

Examples of aminoacid sequences of predominant forms of human histones are listed in Fig. 1 [11,12].

H1, the linker histone, contains only a few carboxylate groups and does not contain any histidine or cysteine residues. There are few potential metal-binding sites in all the histone sequences. Several histidine residues in H2, H3 and H4 and only few cysteine residues in H3 protein can be found. From X-ray crystal structure of the nucleosome, the histidine and cysteine residues in H2 and H3 are, however, in most cases located in the inner part of the protein (Fig. 2) [13,14].

Researchers first addressed their attention to H3, mostly because of the presence of cysteine and histidine residues in its sequence; then, because of the N-terminal tail accessibility by metal ions, to H4 histone. The search for the binding sites has been completed with some motifs on H2A and H2B especially because of the oxidative and hydrolysis potential of some of its metal coordinated portions.

The authors began their studies by using small peptide fragments as models of the histone octamer; the N- and C-ends of the model peptides were respectively, acetylated and amidated in order to obtain more appropriate models of the proteins.

In fact, a great deal of information can be obtained by using small fragments as model peptides; they can provide easier systems to be studied by both experimental and theoretical techniques.

A histidine located in position 18 from the N-terminus is present in the histone H4 tail that extends from the core, where it can be accessible for metal interaction. An $A_{15}KRH_{18}RK_{20}$ motif, as a minimal model of the entire H4 protein, has then been studied [15–19].

On H3 protein only, cysteine residues are present; a $C_{110}AIH_{113}$ motif [20–22], containing a cysteine and a histidine residue, has been chosen as a minimal model of H3; although it is located inside the protein, near to a twofold symmetry axis of the octamer, [23–25], the motif appeared to be accessible. As a matter of fact, it is the binding site for Hg(II) in octamer crystals used for X-ray measurements [23,24].

To verify whether $A_{15}KRH_{18}RK_{20}$ and $C_{110}AIH_{113}$ motifs can remain as the Ni(II) binding sites in the protein environment, the entire H4 protein [15–19] and the core tetramer $(H3\text{-}H4)_2$ [20–23] have also been studied for metal binding.

Other different motifs, minimal models of H4 ($T_{71}YTEH_{75}A_{76}$) [26], H2A ($T_{120}ESH_{123}H_{124}K_{125}$, plus derived cleaved peptides) [27–34] and H2B ($P_1EPAKSAPAPKKGSKKAVTKAQKKDGKKRKR_{31}$ [35], $N_{63}SFVNDIFERIAGEASRLAH_{82}YNKRSTITSRE_{93}$ [36], $I_{94}QTAVRLLLP\ GELAKH_{109}AVSEGTKAVTKYTSSK_{125}$ [37] and $E_{105}LAKH_{109}A_{110}$ [38] have also been studied as nickel binding sites. The complexed species have been tested for specific activity which could be of interest if metal complexes formed inside the cell as a result of nickel exposure.

The aim of the present review is to provide a comprehensive overview of literature dealing with nickel coordination to histone proteins and its link with nickel involvement in toxicity and carcinogenicity.

2.1. Motifs from histone H4 protein

2.1.1. $A_{15}KRH_{18}RK_{20}$, $S_1GRGKGGKGLGKGGAKRH_{18}RKVL_{22}$, $S_1GRGKGGKGLGKGGAKRH_{18}RKVLRDNIQGIT_{30}$ and $T_{71}YTEH_{75}A_{76}$

AKRHRK motif, located in the N-terminal tail of histone H4, has been proposed as a site for nickel binding mostly because of the accessibility of its tail and, as a consequence, of the inhibitory effects of nickel on the acetylation of lysine residues close the His residue. [39]

In fact, nickel, at non toxic concentration, decreases the levels of histone H4 acetylation *in vivo* in both yeast and mammalian cells, with a difference between the two species, as all the four lysine residues were affected in the former and only lysine 12 in the latter. Moreover, lysine 12 and 16, in yeast, are more greatly affected than lysine 5 and 8. Interestingly, a Ni(II) anchoring site has been found at position 18 from N-terminal tail of H4: a histidine residue.

No inhibition of acetylation level by nickel occurs, under the same assay conditions, with histone H3.

These data support the assumption that following nickel binding to histidine 18 of histone H4 *in vivo*, the addition of acetyl groups to the nearby lysine residues has been prevented.

The histone H4 N-terminal tail can be post-translationally modified by acetylation, extending out of the core and therefore being

Fig. 1. Sequences of the predominant form of human histones. Histidine and cysteine residues are underlined in green and orange color, respectively.

accessible for metal binding. For this reason, AKRHRK which is the 6-aminoacid minimal motif, the 22- and 30-aminoacid, the entire tail sequence, and finally the entire H4 protein have been studied for nickel binding. The 7- and 11-aminoacid motifs, Ac-AK(Ac)RHRK(Ac) and Ac-GK(Ac)GGAK(Ac)RHRK(Ac), respectively, in which all lysine residues side chains were acetylated, were investigated in order to verify whether lysine acetylation actually influences their coordination behavior.

Potentiometric and spectroscopic analysis (UV–vis, CD and NMR) showed that histidine acts as a metal anchoring site.

Ni(II) coordination started at pH = 5 by involving the imidazole nitrogen. Five complex species are then formed, from the minor NiH_2L, which is an octahedral 1N species up to $NiH_{-1}L$, $NiH_{-2}L$, $NiH_{-3}L$, which are square planar 4N species.

The distribution diagram for a 1:1 system of Ni(II) (1×10^{-3} mol dm^{-3}) with Ac-AKRHRK-Am is reported in Fig. 3; it shows that, by increasing the pH, nickel ions promoted deprotonation of successive peptide nitrogen atoms, forming Ni-N$^-$ bonds until, above pH 8, the formation of $NiH_{-3}L$, which is a 4N species, was obtained. As it is possible to see from Tables 1 and 2, although the imidazole nitrogen in the H4 model was up to one order of magnitude more acidic than that of some comparable peptides, in this case the stability constant for the Ni(II)-4N complex was considerably higher: log K^* = −28,70 for Ac-AKRHRK-Am compared with log K^* = −30.02 for Boc-AGGH fragment.

Significant downfield and upfield shifts, upon complexation, especially regarding the H_α protons of the backbone, can be seen in the NMR spectra (Fig. 4).

Alanine H_α signal experienced a strong downfield shift with a $\Delta\delta$ = +0.11 ppm for the resonance at 1.93 ppm in the free peptide, suggesting that structural changes occurred at the N-terminal tail after complexation.

Furthermore, while arginine H_δ protons were not affected by the metal, lysine H_ε protons were downfield shifted, implying changes in the hydrophobic packing of side chains of lysine residues.

A comparison between the binding behavior of AKRHRK motif and of the aminoacid Ac-AK(Ac)RHRK(Ac) and Ac-GK(Ac)GGAK(Ac)RHRK(Ac) fragments, where all lysine residues side chains are acetylated, was also reported [16].

The 22-aminoacid motif starts to bind Ni(II) at a slightly higher pH, around 7, involving the imidazole nitrogen of histidine by forming a 1N complex. By increasing the pH, as for the minimal fragment, Ni(II) ions deprotonate successive peptide nitrogen atoms forming M-N$^-$ bonds until a 4N species was detected (Fig. 5).

Table 1
Stability constants of complexes of H^+ and Ni^{2+} with Ac-AKRHRK-Am and comparable ligand at 298 K and I = 0.10 mol dm^{-3} (KNO_3).

Protonation constants (log values)	β(HL)	$\beta(H_2L)$	$\beta(H_3L)$	K_{imid}	KNH_2Lys	KNH_2Lys
Ac-AKRHRK-Am	11.03 ± 0.01	20.90 ± 0.01	27.03 ± 0.01	6.13	9.87	11.03
Boc-AGGH[38]	7.19	10.02		7.19		

Nickel complexes stability constants (log β values)	NiH_2L	NiHL	$NiH_{-1}L$	$NiH_{-2}L$	$NiH_{-3}L$
Ac-AKRHRK-Am	23.01 ± 0.06	15.05 ± 0.04	−1.67 ± 0.01	−11.80 ± 0.02	−22.84 ± 0.03
Boc-AGGH[57]			−4.49		−22.83

Log K^*	1N	2N	4N
Ac-AKRHRK-Am	−4.02	−11.98	−28.70
Boc-AGGH [57]		−11.68	−30.02

Reproduced from Ref. [15], copyright 2000, with permission from Elsevier.

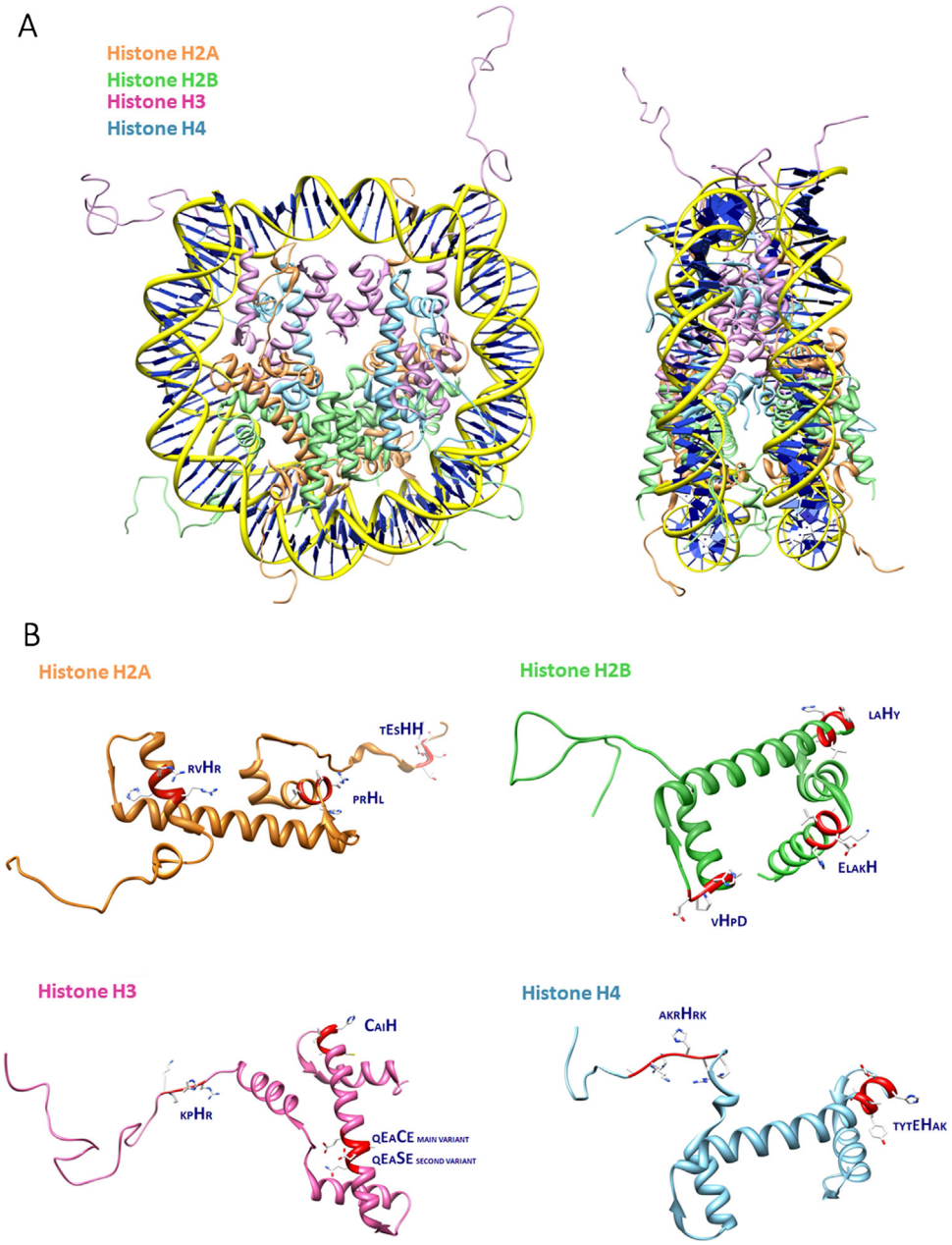

Fig. 2. (A) Nucleosome core particle: ribbon traces (yellow) for the 146-bp DNA phosphodiester backbones (nucleobases blue colored) and eight histone protein main chains (pink: H3; cyan: H4; orange: H2A; green: H2B). The views are from below the DNA superhelix axis for the left particle and perpendicular to it for the right particle. For both particles, the pseudo-twofold axis is vertically aligned with the DNA center at the top; (B) potential binding sites in histone H2A, H2B, H3 and H4. The structures were generated with UCSF Chimera [13] using the PDB entry 1KX5: *X-Ray Structure of the Nucleosome Core Particle, NCP147, at 1.9 A Resolution* [14].

The driving force of the coordination process, as usually encountered for such a peptide pattern, is the formation of stable five-membered chelate rings. The process is not considerably influenced by lysine acetylation. The thermodynamic constants for 3N and 4N species with the 22-aminoacid fragment were higher than those of simple peptides as Boc-AGGH fragment, where glycines instead of arginine or lysine residues were present close to the anchoring site, $\log K^* = -28.67$ for 4N species of the 22-aa peptide of H4 tail and $\log K^* = -30.02$ for 4N species of Boc-AGGH peptide.

Nickel interaction with the 22-aminoacid fragment, Ac-SGRGKGGKGLGKGGAKRHRKVL-Am, and its complexes have been studied by using techniques such as X-ray absorption spectroscopic (XAS) including XANES and EXAFS, X-ray absorption near-edge spectroscopy and extended X-ray absorption fine structure, respectively [18].

Examination of the Ni K-edge XANES spectrum (Fig. S1, Supplementary materials) demonstrated only a weak peak due to the $1S \rightarrow 3d$ electronic transition (peak area $2.6(5) \times 10^{-2}$ eV), with the absolute lack of any peak associated with a $1s \rightarrow 4p$ electronic transition, diagnostic of a planar, low spin, Ni tetra-aza complex in a four coordinated geometry, as noted in all previous measurements. It thus seemed clear that the nickel complex formed by this peptide under the condition used for XAS analysis was a six coordinate species. EXAFS analysis showed the presence of six O- or N-donors around the metal, with 2.06(2) Å as an average Ni-O/N distance. The structure obtained is consistent with a coordination pattern bearing four ligands acquired from the peptide and the remaining two from water molecules. EXAFS multiple scattering analysis deriving from atoms in the second and third coordination sphere of Ni(II) helped cast more light on the nature of the complex

Table 2
Stability constants of complexes of H^+ and Ni^{2+} with Ac-SGRGKGGKGLGKGGAKRHRKVL-Am, Ac-AK(Ac)RHRK(Ac)V-Am and comparable ligand at 298 K and $I = 0.10$ mol dm^{-3} (KNO_3).

Protonation constants (log values)	HL	H_2L	H_3L	H_4L	H_5L	H_6L
Ac-SGRGKGGKGLGKGGAKRHRKVL-Am	11.79 ± 0.10	22.54 ± 0.06	32.62 ± 0.09	42.65 ± 0.07	51.85 ± 0.08	57.84 ± 0.08
Ac-AK(Ac)RHRK(Ac)V-Am	6.08 ± 0.01					
Ac-TRSRSHTSEGTRSR-Am[55]	6.35	10.36				

Nickel complexes stability constants (log β values)	NiH_4L	NiH_3L	NiH_2L	NiHL	NiL	$NiH_{-1}L$	$NiH_{-2}L$	$NiH_{-3}L$	$NiH_{-4}L$
Ac-SGRGKGGKGLGKGGAKRHRKVL-Am	45.50 ± 0.05	37.15 ± 0.06	29.17 ± 0.01	19.98 ± 0.01	10.00 ± 0.02	−0.16 ± 0.02	−10.78 ± 0.02	−21.98 ± 0.02	
Ac-AK(Ac)RHRK(Ac)V-Am					2.62 ± 0.06	−5.34 ± 0.05		−22.12 ± 0.03	−33.37 ± 0.01
Ac-TRSRSHTSEGTRSR-Am [55]					2.73		−13.47	−21.81	

Log K^*	1N	2N	3N	4N
Ac-SGRGKGGKGLGKGGAKRHRKVL-Am		−12.34	−20.69	−28.67
Ac-AK(Ac)RHRK(Ac)V-Am	−3.46	−11.42		−28.20
Ac-TRSRSHTSEGTRSR-Am[55]	−3.62		−19.82	−28.16

Reproduced from Ref. [16] with permission from The Royal Society of Chemistry.

confirming that one His ligand is directly bound to nickel with 4.26(5) Å as an average Ni-C/N distance at the second coordination sphere. The different results obtained from this experiment with respect to previous data gathered from potentiometric and spectroscopic measurements can be explained by the different conditions used to record XAS spectra. In fact, the Ni-peptide complex for the latter analysis was prepared by dissolving the peptide in deionized water containing also 20% glycerol, followed by addition of a $NiCl_2$ solution until a 1:1 ratio of $NiCl_2$/peptide was reached. The presence of 20% glycerol in the complex solution can make the difference, in that glycerol can displace nitrogen donors from the backbone of the peptide.

The pK_a value calculated for N_ε imidazole nitrogen of histidine residue of the "tail" and of the models are, in the range 5.99–6.13, of the same order of magnitude. They are more acidic, about one order of magnitude, than other simple peptides reported for comparison, such as, for example, Boc-AGGH, Ac-GGGH, Ac-GGH, which have 7.19, 7.21 and 7.18 pK_a values, respectively.

pK_a(NH_{im}^+) values for the motifs studied are of the same order of magnitude than those for N-terminal free peptides and bearing electron-withdrawing groups at the pyrrolic nitrogen [40]. The lower basicity could be related both to the electrostatic effect of the positive charge from NH_3^+ terminus as well as to the inductive effect of the substituting groups. The same effect, the lower basicity found in the model of H4 tail, can be related to the electrostatic effect due to the positively charged arginine and lysine side chains present in the peptide sequences. The stability constants, as log K^* values for 1N complexed species (at N_ε of imidazole) of acetylated peptides are linearly connected with the pK_a(NH_{im}^+) of the free peptides [41]. The labilizing effect of the metal ions on the peptide protons is greatly related to the extent of electron donation exerted by the group which acts as the initial coordination site. Thus, a lower degree of electron donation to the metal ion will involve a lower pK_a(NH_{im}^+), which

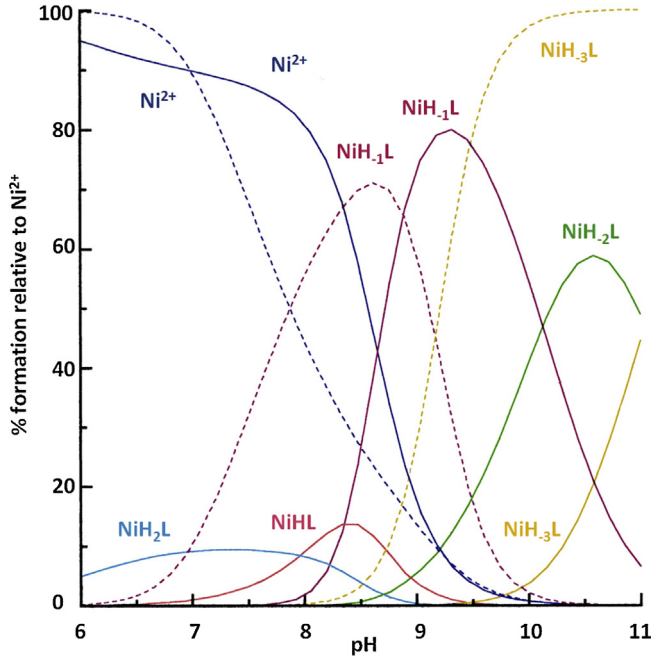

Fig. 3. Comparison of the distribution diagrams of the species for a 1:1 mixture of Ni(II) with Ac-AKRHRK-Am (filled line) and Ni(II)-Boc-AGGH species (dashed line). Reproduced from Ref. [15] copyright 2000, with permission from Elsevier.

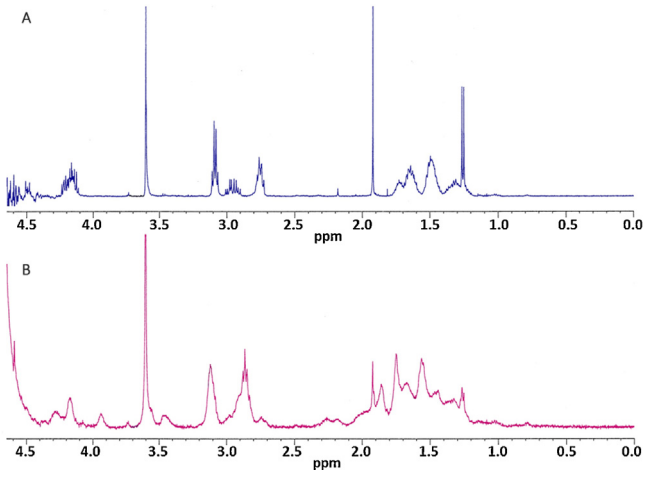

Fig. 4. The 500 MHz ^{1}H NMR spectra of (A) Ac-AKRHRK-Am and (B) Ac-AKRHRK-Am-Ni(II) complex at pH = 9.4.
Reproduced from Ref. [15] copyright 2000, with permission from Elsevier.

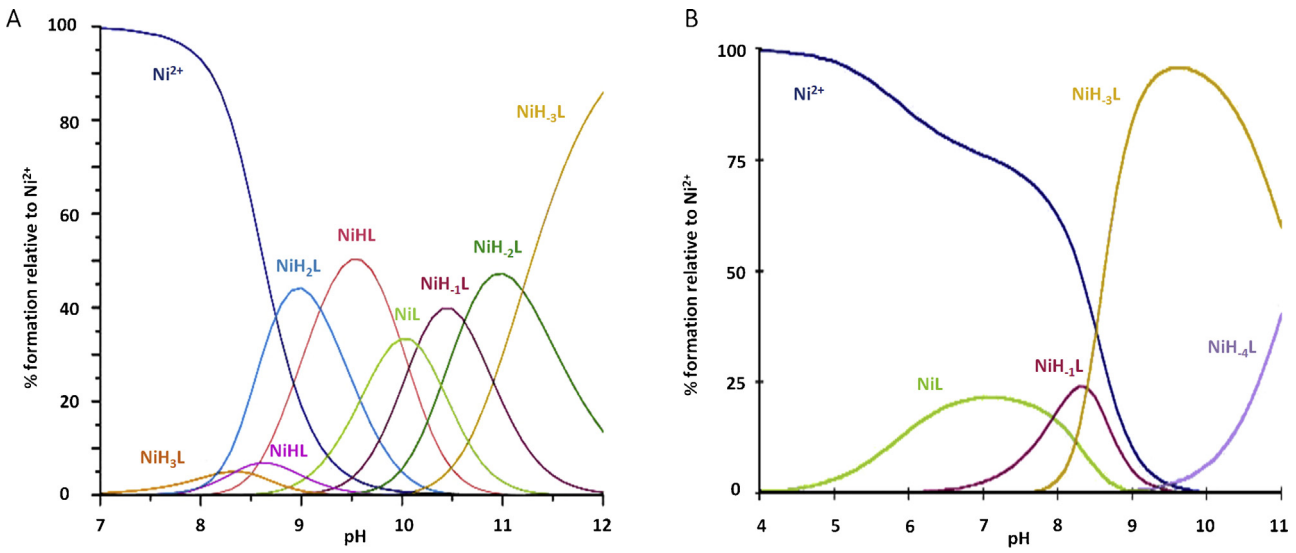

Fig. 5. Species distribution curves for Ni(II) complexes of (A) Ac-SGRGKGGKGLGKGGAKRHRKVL-Am and (B) Ac-AK(Ac)RHRK(Ac)V-Am, in a 1:1 Ni(II)-to-peptide molar ratio. Reproduced from Ref. [16] with permission from The Royal Society of Chemistry.

will be associated with a lower pK_a(amide) value, as reported in Table 2.

Hence, the lower the basicity of N_ε, the simpler will be the deprotonation of amide nitrogen atoms, promoted by metal ions, which results in an increase of π-electron contribution to the metal–amide nitrogen bond when compared with Boc-AGGH or other simple peptides [42]. In addition, the inverted order of log K^* obtained for 3- and 4N species with the tail when compared with the values obtained for similar species with Boc-AGGH or other simple peptides, can also derive from this behavior. The order obtained pK_{am3} < pK_{am2} value indicates that the deprotonation of the second peptide nitrogen happens at a lower pK_a than the first, that is the characteristic of a cooperative coordination process usually found in the peptide coordination mode [10]. The involvement of the secondary peptide structure has to be considered in the stability of the complex [43]. The fully protonated and deprotonated form of the "tail" have qualitatively similar CD spectra which closely resemble those of unordered peptides. While motifs with acetylated lysine residues and with Cu(II) [16] do not show changes in the CD spectrum, a clear feature, with an observed $\Delta\varepsilon$ value of about 5 mol cm^{-1} dm^{-3} in the 220–230 nm region dominated by the peptide carbonyl chromophore, has been detected in the Ni(II)-4N species with the tail [44,45]. A bent structure with an organization of side-chain orientation promoted by the coordination of Ni(II), can be suggested. At the reported experimental conditions, the nickel complexation at a physiological pH is not very effective, but a higher specificity of Ni(II) to cause a peculiar conformation of the peptide may result, somehow paradoxically, from the formation of a rigid square planar complex [43]. Furthermore, a site-selective association of the tail Ni(II) coordinated with the negatively charged DNA backbone can result from the presence of positively charged residues near the metal binding site in the H4 tail [46,47]. Several hydrophobic portions inside the protein should increase the metal binding abilities especially stabilizing the interaction, as reported in the literature [48–50].

The conformational behavior upon Ni(II) coordination is dependent on the chain length, although the coordination ability with the entire tail is similar to that in the smaller AKRHRK motif. Actually, Ni(II) coordination to the 22- or to the 30-SGRGKGGKGLGKGG AKRHRKVLRDIQGIT amino acid peptide, the entire histone H4 tail, induces organization of side-chain orientation, differently from Cu(II) [16] and from motifs with acetylated lysine residues. The data obtained with Ni(II) ions showed that H4 amino-terminal tail can adopt different conformations depending on the metal ion. All these facts may be physiologically relevant to the mechanism of nickel carcinogenesis.

Concluding, histidine 18 residue, behaving as a primary binding site for Ni(II) ions, makes H4 tail an important site which can potentially be involved in the biological activity of nickel.

The coordination properties of the tail have also been studied by using mono and multidimensional NMR techniques (1D, 2D TOCSY, 2D NOESY) [19].

The behavior of His_{18} ring proton signals, studied through ^{1}H NMR, by following the effect of incremental addition of Ni(II) ions, has demonstrated progressive saturation of the binding site by the metal. In the region between 6.5 and 8.0 ppm, $H_{\varepsilon1}$ and $H_{\delta2}$ resonances only were visible, as expected. By addition of the metal, two new peaks progressively appeared upfield with respect to the former ones, corresponding to the same proton resonances now in the new environment generated by metal coordination. The signals of the free histidinic protons, at 1:0.8, peptide:Ni molar ratio, disappeared and only those of the coordinated species were visible. By the addition of 1 equivalent of Ni(II), the trend of the peak height (data not reported), in absolute, for $H_{\varepsilon1}$ proton on His_{18} ring *vs* the equivalents of Ni(II) added, showed that this signal reached about 90% of the maximum of the intensity. This result points out that His_{18} has a relatively high affinity toward Ni(II), binding it in a ratio near to 1:1 (Fig. 6).

The proton signals from Lys_{16}, Arg_{17}, His_{18} and Arg_{19}, experience a shift with respect to their position in the free ligand, after Ni(II) addition (Fig. 7), indicating that this is the region of the peptide mostly involved in the coordination process.

The strong upfield shifts observed for $H_{\varepsilon1}$ proton signals of His_{18} together with H_α of His_{18}, Arg_{17} and Lys_{16}, point to a coordination set involving $N_{\delta1}$ from the imidazoline ring of His_{18} and the amidic nitrogen atoms of these three residues from the peptide backbone. The most striking aspect of the Ni(II)–peptide complex has been demonstrated by the behavior of Lys_{16} signals: its α proton is strongly shielded following amide deprotonation and nickel binding, whereas all the remaining protons undergo evident downfield shifts whose $\Delta\delta$ decreased according to the order $\beta > \gamma > \delta > \varepsilon$. Moreover 2D NOESY spectra registered a set of NOE cross-peaks for histidine $H_{\varepsilon1}$ proton following nickel coordination, as reported in Fig. 8. By the inspection of the recorded cross-peaks an interaction between histidine H_ε and all the aliphatic protons from lysine side chain (see Table 3) can be easily seen, making clear that

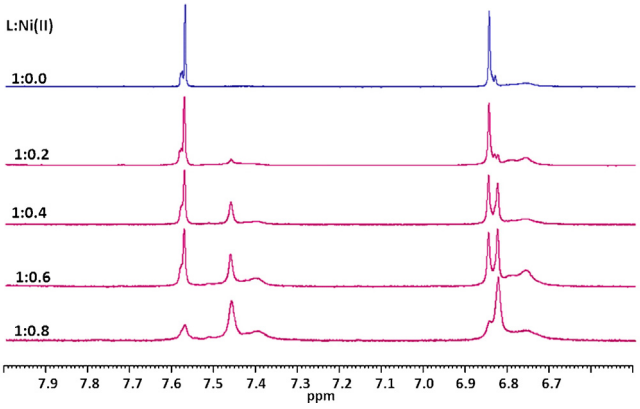

Fig. 6. Aromatic region of 600 MHz 1D NMR spectra of Ac-SGRGKGGKGLGKG-GAKRHRKVLRDNIQGIT-Am peptide with increasing amounts of Ni(II) from 0 eq. (free peptide) to 0.8 eq.

Reproduced from Ref. [19] with permission from The Royal Society of Chemistry.

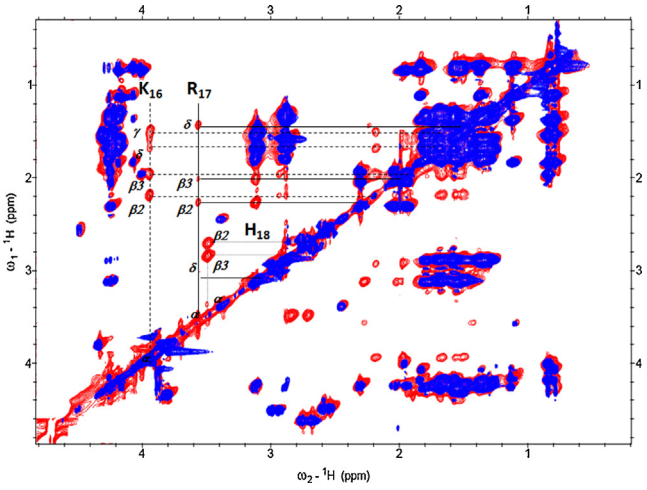

Fig. 7. Overlaid aliphatic region of the 2D ^{1}H–^{1}H NMR TOCSY spectra for Ac-SGRGKGGKGLGKGGAKRHRKVLRDNIQGIT-Am free peptide (blue) and Ni(II) bound peptide (red) at a 1:0.8 peptide-to-nickel molar ratio. New resonances due to Ni-binding have been labeled.

Reproduced from Ref. [19] with permission from The Royal Society of Chemistry.

Lys_{16} should directly point toward the histidine residue by passing over the plane of coordination.

The NOEs observed in 2D NOESY spectra showed an interaction of both $H_{\varepsilon 1}$ and $H_{\delta 2}$ with the aliphatic protons of Lys_{16} and Arg_{17} side chains, demonstrating at the same time the new connectivities between these two residues. A new set of cross-peaks emerged, in the aliphatic region of the spectra, also for H_α and H_β aliphatic protons of His_{18} correlated to the side chain protons of Lys_{16}, Arg_{17} and Arg_{19}; these cross-peaks were not visible in the TOCSY spectra obtained under the same conditions. Some further NOE peaks set at 0.832 ppm and 0.837 ppm have been attributed presumably to the interaction of the aromatic histidine protons with the aliphatic $Q_{\delta 1}$ and $Q_{\delta 2}$ signals of leucine residues, respectively.

It is evident that the three-dimensional geometry of histone H4 N-terminal tail undergoes a great degree of spatial conformational changes due to nickel coordination, as confirmed by the complex structural model, calculated from NOEs recorded for Lys_{16}, Arg_{17}, His_{18} and Arg_{19} residues (Fig. 9).

Fig. 9A and B reports a superposition of the backbones of the structures, for the Ni(II) complex, that are the best 20 selected with lowest overall energy, together with the minimized average structure for which the optimization of molecular mechanics geometry

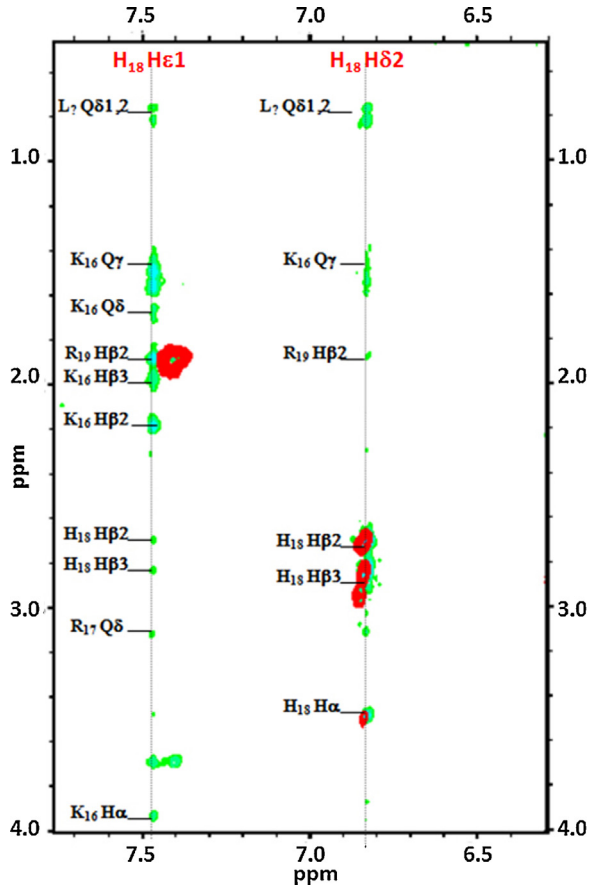

Fig. 8. Overlaid aromatic 2D ^{1}H–^{1}H NMR NOESY (green) and TOCSY (red) spectra of Ni(II)-bound Ac-SGRGKGGKGLGKGGAKRHRKVLRDNIQGIT-Am peptide at a 1:0.8 peptide-to-nickel molar ratio.

Reproduced from Ref. [19] with permission from The Royal Society of Chemistry.

was calculated. The calculated models show that Lys_{16} and Arg_{17} residues extend above the coordination plane while Arg_{19} lies under it, extending downwards and far from the metal. Lys_{16} side chain reaches over the metal center leaning toward the imidazolic ring, while Arg_{17}, pointing upwards, is slightly tipped up toward the ring too. This disposition of the two side chains covers the upper face of the plane of coordination, protecting it from the attack of water molecules and then stabilizing the complex. The conformational changes occurring in the Lys_{16} side chain can be of critical

Table 3
Inter-residual constraints allowing for structural analysis of the Ni(II)-peptide complex.

Residue 1	Proton 1	Residue 2	Proton 2	Upper limit distance (Å)
Lys_{16}	$H\alpha$	His_{18}	$H\varepsilon_1$	4.85
Lys_{16}	$H\alpha$	Arg_{17}	$H\alpha$	4.57
Lys_{16}	$H\beta_2$	His_{18}	$H\varepsilon_1$	4.20
Lys_{16}	$H\beta_3$	His_{18}	$H\varepsilon_1$	3.95
Lys_{16}	$Q\delta$	Arg_{17}	$H\alpha$	4.27
Lys_{16}	$Q\delta$	His_{18}	$H\varepsilon_1$	4.74
Lys_{16}	$Q\gamma$	His_{18}	$H\varepsilon_1$	3.64
Lys_{16}	$Q\varepsilon$	His_{18}	$H\varepsilon_1$	5.66
Arg_{17}	$Q\delta$	His_{18}	$H\varepsilon_1$	5.04
His_{18}	$H\beta_2$	Arg_{19}	$H\beta_2$	4,57
His_{18}	$H\varepsilon_1$	Arg_{19}	$H\beta_2$	3.93
His_{18}	$H\varepsilon_1$	Arg_{19}	$H\beta_3$	3.95
His_{18}	$H\delta_2$	Arg_{19}	$H\beta_2$	5.45
His_{18}	$H\delta_2$	Arg_{19}	$H\beta_3$	6.08
His_{18}	$H\delta_2$	Arg_{19}	$Q\delta$	5.38

Reproduced from Ref. [19].

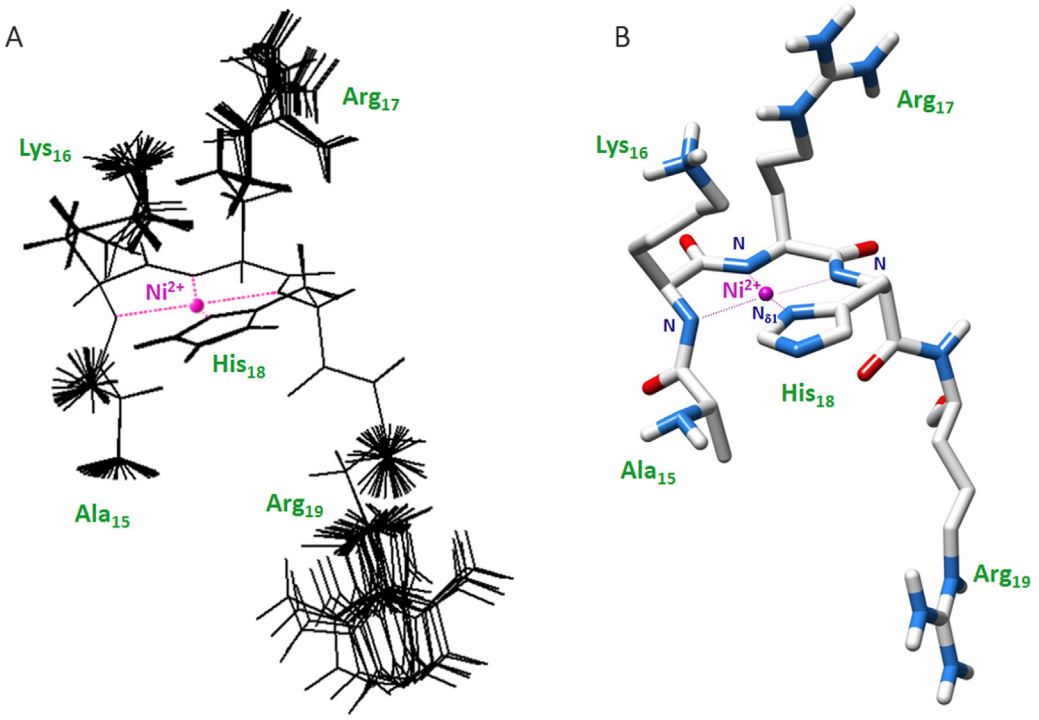

Fig. 9. (A) Superposition of the 20 lowest energy structures of the AKRHR peptide fragment bound to Ni(II) obtained from NMR data. (B) Relative minimized average structure of the family. The 3D structure was generated with UCSF Chimera program [13].
Reproduced from Ref. [19] with permission from The Royal Society of Chemistry.

importance in the enzyme recognition processes, *i.e.* in the acetylation event led by the HAT (acetyltransferase) enzyme on lysine itself. In fact, Lys_{16} is located at the same time in the region near to histidine H_{18}, which is the focus of nickel binding on histone H4, and in the center of a likely recognition motif for HAT enzyme, composed by a 6–7 amino acid fragment [51,52].

Different studies have provided evidence that this particular portion of histone H4 should be set, in an extended conformation, inside a cleft on the enzyme, in that the recognition of the substrate and the acetylation of lysine residues happen; so that any conformational variation on Lys_{16} or on a part of the recognition motif caused by nickel binding, might hinder HAT enzyme activity inducing transcription errors and subsequent DNA impairments [53].

2.1.1.1. $T_{71}YTEH_{75}A_{76}$. Histone H4 bears another histidine residue in the C-terminal region. Although it lies inside the nucleosome core, the coordination ability of Ni(II) toward a six amino acids fragment, TYTEHA, containing a histidine residue at the 75th position in the C-terminus, was studied by means of a combined pH-metric and spectroscopic (UV–vis, EPR, CD and NMR) investigation [26], in order to get more information and to suggest possible *in vivo* pathways involved in nickel carcinogenesis.

The coordination properties of the fragment resemble the typical binding motifs of Ni(II) complexes when a His residue is located in an internal position of the sequence.

At physiological pH, the formation of an octahedral macrochelate species, involving N_{Im} and O_{Glu} donors in the coordination (Fig. 13A), was clearly demonstrated by the low intensity of d–d bands in the CD spectrum. Its stability constant ($\log\beta = 13.72$) value is comparable to those of similar Ni(II) species (Ni-ELAKHA, $\log\beta = 13.24$; Ni-TESAHK, $\log\beta = 13.02$; or Ni-TRSRSHTSEGTRSR, $\log\beta = 13.98$) [31,38,58].

In particular, the presence of a Thr residue close to the coordination site in TYTEHA motif is significant for the nickel-mediated hydrolysis process [28–34]. In fact, the formation of the Ni-4N (N_{Im},$4N^-$)-TYTEHA species, at pH 9 (Fig. 13B), was accompanied by hydrolytic cleavage and formation of a square planar complex. The Tyr-Thr peptide bond hydrolysis resulted in the formation of $TY\text{-}COO^-$ fragment and the complexed Ni(II)-TEHA species.

The hydrolytic abilities of Ni(II) ions toward this sequence, located in the C-terminus of H4, may cause damage to the entire nucleosome.

2.1.2. Histone H4 protein

Recent literature data have reported that acetylation on lysine residues located on N-terminal tail of H4 increases the extent of α-helical conformation [51], causing a shortening of the tail that may have important structural and functional roles as a part of transcriptional regulation mechanism. Actually, nickel induces a secondary structure in the protein H4 [54]. More specifically, as demonstrated from a circular dichroism study, it promotes an increase in α-helical conformation of the non-acetylated histone H4, which is, indeed, the same effect as acetylation.

Nickel shows a preference for specific lysine residues highly conserved in the H4 N-terminal tail $S_1GRGK_5{}^*GGK_8{}^*GLGK_{12}{}^*GGAK_{16}{}^*RH_{18}RKVL_{22}$ (asterisks pinpoint the sites of acetylation in the sequence), where the sites of acetylation are grouped. Not all lysine residues are acetylated in the same way: the decrease in the acetylation degree differed in extent with lysine residues occurring at positions 5, 8, 12 and 16, being Lys_{12} and Lys_{16} the most sensitive residues. Two cell generations incubated with 1 mM $NiCl_2$ were in fact able to inhibit acetylation at these positions.

The spacing between acetylable lysine residues is remarkably regular in the amino termini of many histones, with lysine residues occurring at positions 5, 8, 12 and 16 in H4. In this way, such a spacing periodicity is "reminiscent of that of an α-helix", that is 3.6 residues; it could be part of the so-called histone recognition motif [55], probably involved also in the acetylation processes that

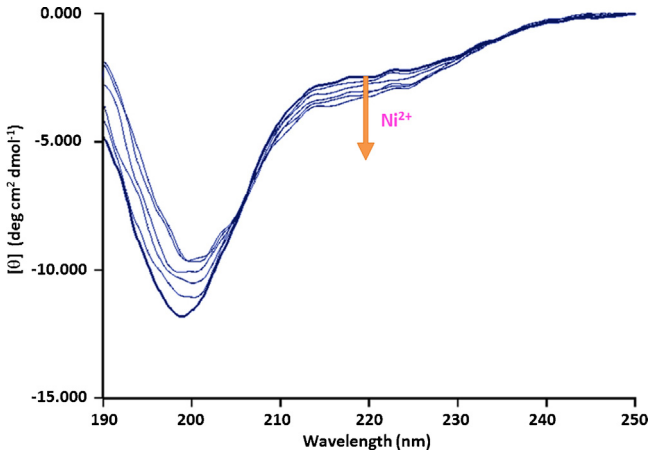

Fig. 10. CD spectra of a solution containing H4 protein and Ni(II) ions at pH 8.7 (5 mM tetraborate/HCl buffer) with increasing nickel concentrations (the thick line refers to metal free histone H4).

Reproduced from Ref. [54] with permission from The Royal Society of Chemistry.

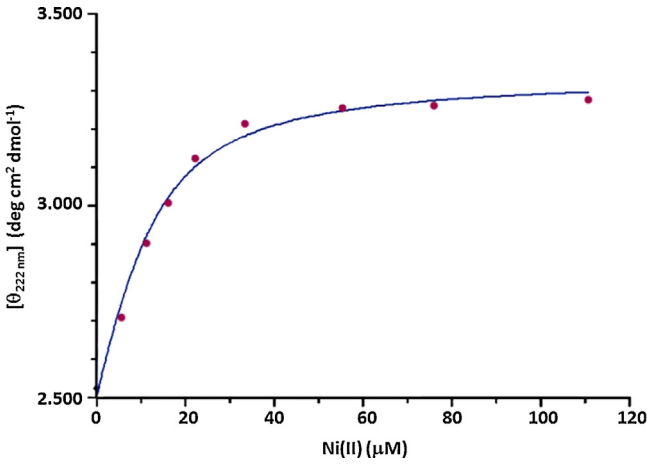

Fig. 11. Dependence of the mean residue ellipticity at 222 nm (absolute value) of a 11 mM solution of H4 as a function of Ni(II) concentration in 5 mM tetraborate/HCl buffer at pH 8.7.

Reproduced from Ref. [54] with permission from The Royal Society of Chemistry.

induce strong structural and conformational changes in histone H4 by increasing the α-helical content on its acetylated N-terminal tail [56]. The tail region going from Ala_{15} to Val_{21} is the most likely candidate for giving rise to the overall H4 α-helical content which was observed either in nucleosome core particles, or in histone octamer and N-terminal H4 tail, after 90% TFE (an effective α-helical stabilizer) addition.

When Ni(II) is not present in solution, a negative band at 200 nm, characteristic of a random coil conformation, is the prevalent CD feature of histone H4 protein. A positive band at about 190 nm, together with two negative bands at 206 and at 222 nm, have been demonstrated in the CD spectra, as Ni(II) was added in slightly basic water at pH 8.7, in the absence of buffer. This feature is indicative of a dramatic increase of α-helical content in the protein. The almost isodichroic point close to 203 nm denotes the presence of a mixed helix-coil conformation, while the effect of nickel on α-helix formation is distinctly evident in the CD spectra recorded at pH 8.7 in 5 mM tetraborate/HCl aqueous buffer solution, reported in Fig. 10, where an intensity increase in the CD bands around 220 nm indicates a more structured protein. The enhancement in the negative ellipticity at 222 nm, following Ni(II) addition, is small but significant and reproducible, indicating an increase of α-helix content; in fact, the random coil conformation possesses an ellipticity which is very low at 222 nm. The data obtained by fitting the CD spectra of the protein, showed that the calculated amount of α-helix contributions to the secondary structure stays below 10% even though in the presence of the metal ion.

The α-helical content would be expected to enhance by increasing the concentration of nickel, as it was indeed observed in the case of nickel binding to the histone effectively influencing the acetylation mechanism. The intensity of the CD bands are consequently influenced by the Ni(II)/histone H4 molar ratio, in such a way that the molar ellipticity at 222 nm *vs* Ni(II) concentration is reported in Fig. 11.

The plot clearly shows that, at a certain point, the binding site is saturated by the metal. The binding constant can be estimated by interpolating the spectroscopic variations at different metal ion concentrations with a binding isotherm which takes into account the presence of one high affinity metal binding site, within the protein, having $K_b = (1.76 \pm 0.32) \times 10^5\ M^{-1}$. The partial precipitation of H4 taking place for long incubation time in the presence of basic buffer solution can be responsible for the relatively high standard deviation. The high value of the obtained binding constant indicates that it takes a very low metal concentration in order to saturate histone H4 site by Ni(II) ion, with a following change in protein conformation.

A model of the helical conformation of the non-acetylated H4 N-terminal tail, bound to Ni(II), was obtained by using molecular modeling and computational chemistry software HyperChem(tm) 8.0.7 [57]. The 3D structure was generated by using UCSF Chimera program [13] (Fig. 12).

2.2. *Motifs from histone H3 protein: $C_{110}AIH_{113}$ motif from histone H3 and core tetramer $(H3\text{-}H4)_2$*

The histone H3 protein contains CAIH, from position 110 to 113, motif which is evolutionarily strictly conserved among animal species [11].

Cys_{110} is the only free thiol in H3 protein and it has often been employed as a chemical labeling site [59]. In addition, Hg(II) bound to Cys_{110} was detected as the only species in the heavy atom labeling process for X-ray determination of the crystal structure of histone octamer [23].

Thus, CAIH motif has been chosen as a minimal model for studying nickel interaction with histone octamer in order to find possible implications for the oxidative damage process of DNA and therefore of the entire chromatin.

Combined UV–vis, CD, NMR spectroscopy and potentiometric measurements have been used to study Ni(II) interaction with CAIH fragment.

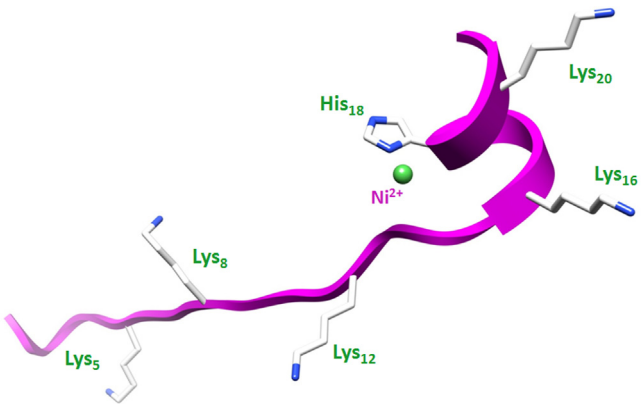

Fig. 12. Molecular-mechanics optimized structure of the helical conformation adopted by the non-acetylated H4 N-terminal tail in the presence of Ni(II) ions.

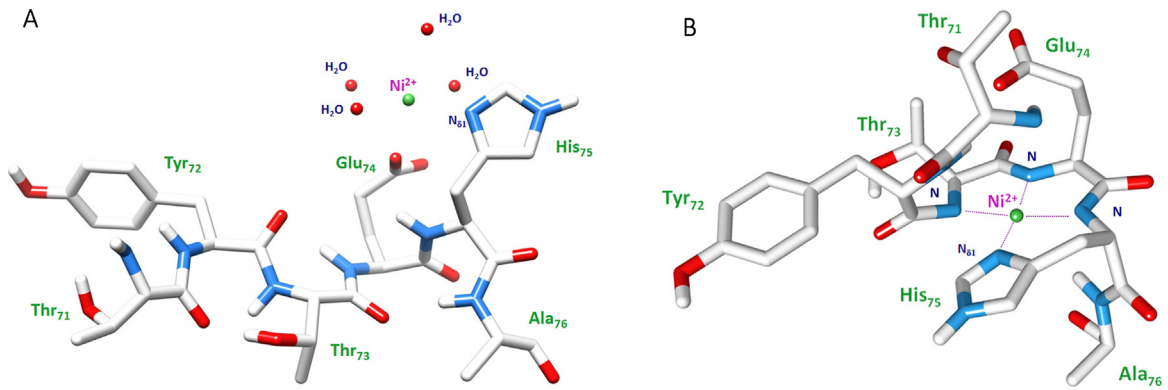

Fig. 13. (A) 3D structural model for the Ni(II) ion complexed with TYTEHA fragment in a octahedral coordination geometry (NiHL), and (B) in a square planar coordination geometry ($NiH_{-2}L$). For the latter the backbone dihedral angles ϕ and ψ of Thr_{73}-Glu_{74}-His_{75} residues and the metal-donor distances were derived from the X-ray structure of the Ni(II)(Glycyl-Glycyl-Alpha-Hydroxy-D,L-Histamine)·$3H_2O$ complex [48]. Models were obtained by molecular modeling and computational chemistry software HyperChem(tm) 8.0.7 [57] and the 3D structure was generated with UCSF Chimera program [13].

CAIH is able to coordinate Ni(II) ions giving, at a physiological pH range, $Ni(CAIH)^+$ and $Ni(CAIH)_2$ complexes obtained at 1:1 and at higher ligand to metal molar ratio, respectively. In both species deprotonated thiol of cysteine and imidazole nitrogen of histidine bind metal ions. CAIH forms an unusual macrochelate loop around Ni(II) ions giving a Ni(II) diamagnetic, low spin species in a distorted square planar geometry (Fig. 14).

The steric crowding between the thiol and the imidazole ring could be responsible for this arrangement which resembles the one detected for other metal complexes with peptides containing histidine residues [40,60,61].

Spectroscopic data are diagnostic of the coordination mode. The d–d band at around 500 and 400 nm, as shoulders, have a very weak CD due to the presence a large macrochelate and the resulting non rigid feature of the conformation [62]; that at 336 nm ($\varepsilon = 5200\ dm^3\ cm^{-1}$) is attributable to a $S \rightarrow Ni(II)$ charge transfer transition. Three $S \rightarrow Ni(II)$ charge transfer transition (S_π, S_π, S_σ, σ and π orbitals of thiolate sulfur, respectively) bands in addition to $N_{Im} \rightarrow Ni(II)$ band can be observed in the CD spectra (348–240 nm range).

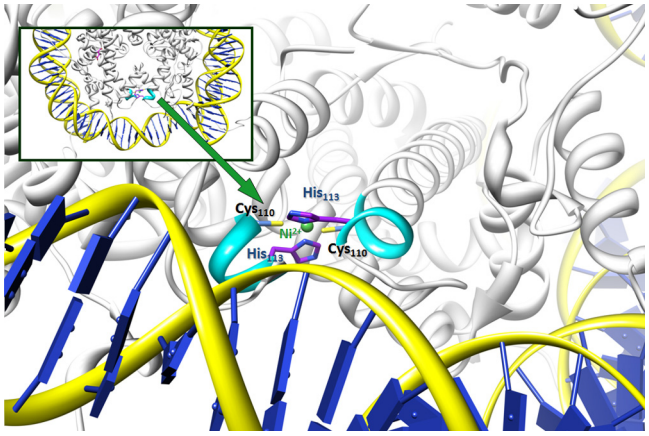

Fig. 14. Model of the potential double nickel-binding site $Ni(CAIH)_2$ in human histone octamer (inset) showing close-up view from the top along the twofold symmetry axis. The model is based on the crystal structure of the Nucleosome Core Particle, NCP147 (PDB entry 1KX5). In the CAIH fragment (cyan colored) of the two H3 histones, the side chains of the Cys_{110} and His_{113} residues were repositioned with appropriate side chain rotamers, followed by addition of Ni(II) ions (green sphere) to yield a pair of metal-binding sites. Structures were generated with UCSF Chimera [13].

Square planar, low spin complexes, as those containing Ni(II) coordinated through thiol donors, are able to generate oxygen-based free radical species.

NMR spectra for $Ni(CAIH)_2$ revealed the presence of spectroscopic lines in two distinct sets from which a fast exchange mode, expressed in terms of NMR experiment time frame, could be involved.

Much broadening and notable shift variations of H_α and H_β proton signals from cysteine residues was observed, while the positions of His $H_{\delta 2}$ and $H_{\varepsilon 1}$ resonances are not much influenced. This seems to indicate that a monodentate binding involving only one cysteine residue, of a second CAIH molecule, could take part in the formation of NiL_2 species. Considering the values of stability constants it has been suggested that the second peptide molecule binds as effectively as the first one.

The dimeric CAIH oxidation product, demonstrated under mild conditions, at a pH value of 7 and in the presence of ambient oxygen, CAIH disulfide, and its weak Ni(II) octahedral complex, rather than monomeric CAIH and its very stable square planar complex, is the major catalysts of 8-oxo-dG (8-oxo-2-deoxyguanosine) formation, at submillimolar concentrations of H_2O_2. Such a weak complex causes the formation of up to 90% of 8-oxo-dG. The mechanism of its action has not so far been investigated.

CAIH disulfide is not capable of binding Ni(II) ions through sulfur atom. This leaves only nitrogen from the imidazole ring as a potential binding site. Evidently, the stability of HIAC-CAIH-Ni(II) cannot be as high as that of $Ni(CAIH)^+$ complex but should rather be comparable to that of nickel imidazole complexes [63].

Thus, it is noteworthy that, although weak and thus often not seriously considered, some nickel complexes may have a peculiar and also very high toxic potential [20]. Nevertheless, the specific chemical mechanism of their reactivity, though certainly interesting, remains to be investigated.

For all the reasons summarized above, Ni(II) coordination to CAIH motif in the core histone H3 may be one of the key event in the oxidative damage of DNA bases, catalyzed by weak Ni(II) complexes and observed in the process of Ni(II) induced carcinogenesis.

Then, the core tetramer $(H3\text{-}H4)_2$ for nickel binding has been studied with the aim of verifying whether CAIH is still able to bind Ni(II) when the motif is inside the protein; the tetramer $(H3\text{-}H4)_2$ has been extracted from chicken erythrocytes [22].

Due to the secondary structure constraints present, at the CAIH site, in $(H3\text{-}H4)_2$ tetramer, Ni(II) is able to bind to a Cys residue from one H3 and a His or Cys residue from another H3 molecule.

The conditional affinity constant for Ni(II) binding, in the tetramer, to CAIH motif at pH 7.4 and for low and high Ni(II)

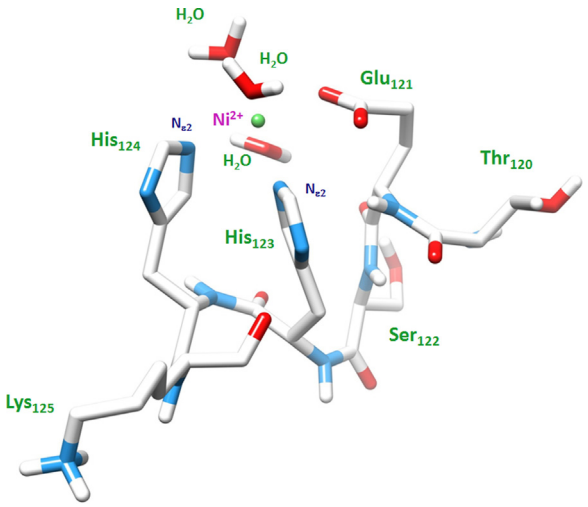

Fig. 15. 3D structural model for the Ni(II) ion complexed with TESHHK fragment in an octahedral coordination geometry (NiHL). The model is obtained by molecular modeling and computational chemistry software HyperChem(tm) 8.0.7 [57] and the 3D structure was generated with UCSF Chimera program [13].

saturation were calculated. The corresponding $\log K^*$ values, 4.26 ± 0.02 and 5.26 ± 0.11 respectively, were obtained from spectrophotometric titration using the charge transfer band at 317 nm, diagnostic of a bond between Ni(II) and sulfur donor from a cysteine, which must be the Cys_{110} residue at the CAIH moiety of histone H3.

Interestingly, a 30-fold stability gain *vs* CAIH model was observed; this could be reasonably due to the shielding exerted by hydrophobic portions present in the interior of the protein.

Therefore, this binding site and its peculiarity must be taken into account in the study of molecular mechanism by which nickel exerts its carcinogenicity.

2.3. Motif from histone H2A: $T_{120}ESH_{123}H_{124}K_{125}$

Histone H2A contains four histidine residues in its 129 amino acid sequence, two of which are adjacent in the C-terminal end of the protein, which is demonstrated to be very important in nickel binding and subsequent hydrolysis, a process that has been often indicated as one of the possible mechanisms behind nickel toxicity [27]. 1D NMR spectra of TESHHK recorded at various pH values allowed to set up a series of titration curves specific to particular imidazole protons. The pK_a values obtained from these curves, are almost identical for both His residues, and their average agrees very well with the average of the corresponding potentiometric values (6.285 and 6.35, respectively).

TESHHK undergoes formation of a pseudo-octahedral NiHL complex in mildly acidic and neutral solutions (pH = 4–7), as confirmed by CD and UV–vis experiments. Ni(II) binds the peptide through the imidazole nitrogen atoms on both its histidine residues and the carboxylate of the glutamic acid side chain (Fig. 15). Calculations devoted to study the complex stabilities indicated that TESHHK motif is a very likely binding site for carcinogenic Ni(II) ions in the cell nucleus. At higher pH, a series of square-planar complexes are formed, above pH 7. At pH 7.4 the peptide hydrolyzes in a Ni(II)-assisted fashion, yielding a square-planar Ni-SHHK-Am complex as the only product detected by CD, MALDI-TOF MS, and HPLC measurements [27].

Further studies revealed that Ni-mediated hydrolysis is about seven times faster with the entire H2A protein and its Ac-LLGKVTIAQGGVLPNIQAVLLPKKTESHHKAKGK model compared with TESHHK peptide studied in the same conditions; in addition a complex, Ni-SHHKAKGK, was the smaller product of the hydrolysis, indicating a high site specificity of the hydrolysis reaction [28,30].

The coordination ability toward Ni(II) ions of SHHK, deriving from TESHHK hydrolysis, has been investigated, to cast light on its stability and coordination [31].

The molecular mechanism of the hydrolysis reaction in Ser-Y-His-X or Thr-Y-His-X fragments where Y and X are any residue but Y = Pro, has been recently reported [116,117]. The hydrolysis starts with the formation of a 4N-Ni(II) species through the coordination of imidazole nitrogen of histidine and the three preceding amidic nitrogen atoms from the backbone. Then, due to the strain exerted by Ni(II) ion on peptidic nitrogen and on side chain, the involvement of the hydroxyl group of Ser or Thr residue as an acceptor of the close acyl moiety occurs. The acyl group is then removed from the amidic nitrogen of Ser or Thr residue and the intermediate ester formed, finally, undergoes the hydrolysis.

A combination of potentiometric and spectroscopic techniques (UV–vis, CD and NMR) suggested that, at pH above 7, the tetrapeptides coordinated equatorially through the imidazole ring of His in position ε, N-terminal amino group and two amide nitrogen atoms located between these two coordinating groups, until a 4N $\{NH_2, 2N^-, N_{Im}\}$ square-planar complex was formed. The d–d band appeared in the UV–vis spectra near 418–421 nm with $\varepsilon = 94–164\ M^{-1}\ cm^{-1}$, together with the CD maxima near 478 and 412 nm of all complexes formed, were in good agreement with the proposed coordination mode [32].

In a final study, the details of metal-assisted histone cleavage have been elucidated. Substitution of the serine residue close to the histidine residues with a threonine residue showed that also in this case hydrolysis was taking place, but the replacement with other amino acids had no effect. Ni(II) complexes with the analogous TETHHK peptide were investigated through potentiometry, electronic absorption spectroscopy and HPLC measurements. The detailed temperature and pH dependence of such Ni(II)-dependent hydrolysis reactions was studied, yielding an activation energy $Ea = 92.0\ kJ\ mol^{-1}$ and activation entropy $\Delta S \neq = 208\ J\ mol^{-1}\ K^{-1}$. The pH profile of the reaction rate coincided with the formation of the four-nitrogen square-planar Ni(II) complex of Ac-TETHHK-NH_2. These results expanded the range of protein sequences susceptible to Ni(II) dependent cleavage by those containing threonine residues and permit predictions of the course of this reaction at various temperatures and pH values [33].

It thus seemed clear that the involvement of a serine or threonine –OH group was necessary for the hydrolytic process to take place.

2.4. Motifs from histone H2B: $P_1EPAKSAPAPKKGSKKAVTKAQKKDGKKRKR_{31}$; $L_{80}AH_{82}YNK_{85}$ and $N_{63}SFVNDIFERIAGEASRLAH_{82}YNKRSTITSRE_{93}$; $E_{105}LAKH_{109}A_{110}$ and $I_{94}QTAVRLLLPGELAKH_{109}AVSEGTKAVTKYTSSK_{125}$

Histone H2B includes different sequences capable of metal binding, some of which contain a histidine as the primary anchoring site for nickel ions; in addition, it contains also lysine residues, at position 4 and 120, which are sites for post-translational modifications such as methylation and ubiquitylation, respectively.

Although its N-terminal end holds no such a residue, nevertheless its sequence can be interesting for metal coordination because it encloses some aspartate and glutamate residues [35]. PEPAKSAPAPKKGSKKAVTKAQKKDGKKRKR, ($H2B_{1-31}$) peptide, end blocked N-terminal tail, has been thus investigated through UV–vis, CD and NMR techniques in its binding to nickel ions. The free peptide, from NMR data, both by chemical shift index (CSI) method and analysis of the low quantity of intermolecular NOE connectivities, showed a random coil conformation in solution. Ni(II) ions begin to bind this sequence at pH higher than 6.7, as shown by the

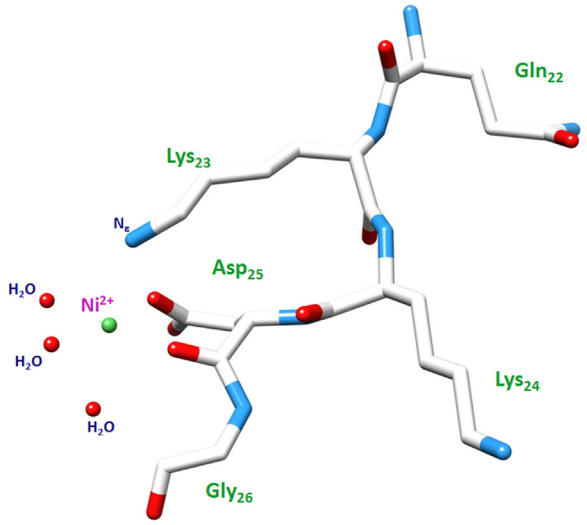

Fig. 16. 3D structural model for the Ni(II) ion complexed with $KQKD_{25}G$ fragment in an octahedral (β-COO^-, ε-NH_2, CO) coordination mode. The model is obtained by molecular modeling and computational chemistry software HyperChem(tm) 8.0.7 [57] and the 3D structure was generated with UCSF Chimera program [13].

presence of a d–d band around 474 nm; up to pH 11.3 a mixture of both diamagnetic and paramagnetic species is present in solution, with the latter definitely more abundant at physiological pH. Actually, in spite of a low band resolution, UV spectra seemed to present, at pH 7.1, a λ_{max} around 382 nm, which is consistent with an octahedral nickel(II) complex [64], although the absorption coefficient ($\varepsilon = 53\ M^{-1}\ cm^{-1}$) was quite high for such a species [65]. The low optical activity of CD d–d transition indicated the presence of mostly paramagnetic species, while the absence of $N_{amide} \rightarrow Ni(II)$ CT transition suggested non-coordination of amide nitrogen atoms, supporting the absence (or small concentration) of square planar complexes around pH 7 [10].

Hence an octahedral species in a (β-COO^-, ε-NH_2, CO) coordination mode could be present, where D_{25} carboxylic moiety, which seems to work as the binder, together with a carbonyl peptide oxygen and an amino group from a lysine or arginine side chain are all involved in the complex formation (Fig. 16).

Successive deprotonation of amidic nitrogen atoms, by raising the pH above 8.2, leads to the appearance of a diamagnetic species predominant at pH above 10; the increase in magnitude of the d–d bands at 423 and 481 nm ($\Delta\varepsilon = -0.21$), together with the CD band at 260 nm, assigned to $N_{amide} \rightarrow Ni(II)$ charge transfer transition [27] and an intense CD d–d band at 416 nm ($\Delta\varepsilon = -0.72$ to $-1.0\ M^{-1}\ cm^{-1}$) all pointed to an amide bond for Ni(II) ions in a square planar environment [10,66].

NMR data and previous observations [67] suggest a very slow kinetics for the switch from the hexacoordinate paramagnetic to the tetracoordinate diamagnetic species. The latter complex thus seems to be formed by four deprotonated amidic nitrogen atoms in a 4N ($4N^-$) coordination mode, namely those relative to the D_{25}, K_{24}, K_{23} and Q_{22} residues [35].

NOE connectivities have been used to calculate a structure in solution for the diamagnetic complex; the results showed a dramatic change in the peptide conformation involving all residues from G_{13} to G_{26}, in order to accommodate the metal ion that is thus able to effectively modify the environment around the binding site. T_{19}, K_{20}, V_{18} and even V_{17} are the most affected residues, together with K_{16}, K_{15}, S_{14} and G_{13} in a minor way but the presence of nickel limits as well the freedom of some other side chains, like K_{20}, thus conferring more rigidity to the peptide. The observed severe conformational change might interfere with histone post-translational modifications, possibly leading to epigenetic effects.

His_{82} and His_{109} histidine residues in histone H2B have been the subject of detailed studies involving more or less extended sequences around them.

ELAKHA and a larger IQTAVRLLLPGELAKHAVSEGTKAVTKYTSSK ($H2B_{94–125}$) portion, including ELAKHA fragment, were investigated as end-blocked peptides in their nickel binding through potentiometric and spectroscopic (NMR, UV–vis and CD) techniques [37,38]. From NMR measurements, on the basis of the NOE connectivities, a well-resolved solution structure for the binding site of the $H2B_{94–125}$-Ni(II) complex was determined. It has thus been observed that nickel binding strongly affects the C-terminal tail of the peptide, forcing it to approach the coordination plane. If such a structural alteration occurs under physiological conditions, it is highly possible that it may interfere with the histone's physiological role and particularly with the ubiquitylation process, taking place at Lys_{120}.

In addition, other different motifs, LAHYNK and a larger NSFVNDIFERIAGEASRLAHYNKRSTITSRE ($H2B_{63–93}$) portion, including LAHYNK fragment, have also been studied as nickel binding sites [68,69].

The coordination properties of all fragments resemble the typical binding motifs of Ni(II) complexes when a His residue is located in an internal position of the sequence.

No breakage of the peptides was demonstrated for all these portions, probably because of the lack of OH-containing residues, like serine or threonine residues, close to the coordination site.

3. Discussion and concluding remarks

Nickel has been proved an essential metal for many archea, bacteria and plants, (for instance, extremely high content of nickel occurs in beans where twelve nickel atoms are present per urease enzyme molecule), but it is believed to be non-essential for humans. The most common oxidation numbers span from 0 to +4; the +2, $3d^8$ electronic configuration, is the only stable oxidation number in simple compounds with nitrogen, sulfur or oxygen as donor atoms. In this state it can adopt different geometries, such as square planar, octahedral, either square pyramidal or trigonal bipyramidal and less common tetrahedral, arrangements. Depending on the ligands strength, structure geometry and then on the energy differences among t_{2g} and e_g d orbitals and their occupation pattern, low- (S = 0), diamagnetic, and high-spin (S = 1), paramagnetic, electron spin states can arise, following the crystal ligand field theory. Other different oxidation numbers require peculiar donor atoms and geometries [70,113].

Nickel metal as well as nickel compounds are of great environmental concern being widely distributed in every day life as well as used in several industrial processes as in refinery, mining and mostly in the producing of all sort of alloys [71–73]. Cell culture, as well as epidemiological and animal studies, have indicated that nickel compounds are carcinogenic, but the molecular mechanisms by which they exert their carcinogenic properties are still uncertain and require additional research [74–77].

Though water soluble nickel compounds have toxic activity, those of low water solubility, comprising oxides NiO_x, either sulfides or sub-sulfides as NiS and Ni_3S_2, exert the most potent activity causing human cancer, especially *via* inhalation.

Nickel insoluble particles enter into cells as they can be phagocytized by them. Once phagocytized, they are included in intracellular vesicles that are localized close to the cell nucleus. The low 4.5 pH inside vesicles dissolves the particles making a continuous source of free Ni(II) ions available. Additionally, following vesicles fusion to the nuclear membranes, Ni(II) ions can be delivered into the nucleus [83–88]. Inside the nucleus, they can selectively

target nucleosome [82] by interacting with specific coordination sites.

Mutation assays, conducted from *Salmonella* to mammalian cells *in vitro*, have demonstrated a relatively low mutagenic activity of nickel compounds; hence the mutagenic activity should not be the key mechanism in nickel induced carcinogenesis [78–81]. Instead, in numerous studies several structural alterations in nuclear chromatin and, as a consequence, epigenetic effects have often been indicated as the primary events in nickel carcinogenesis together with oxidative damages and then genotoxic effects.

Numerous studies converge now and point to the clear evidence that the ability of Ni(II) to bind to specific motifs on nuclear histone proteins could be a key element in the mechanism of its activity. It could potentially disrupt the structure and function of the nucleosome [21,22,27,28,89,90] and then its peculiar complexed species may be able to cause much damage including oxidative DNA lesions thus disturbing gene expression and then resulting in carcinogenicity [90].

Here we described the interaction of nickel with nuclear histone proteins which are believed to be excellent candidates, inside the cell nucleus, for nickel binding.

Considering that studying and characterizing the possible interactions of metal ions with such a big and complex molecule as the histone octamer could be a very difficult undertaking, researchers have, till now, mostly devoted their attention on small fragments which could resemble the binding capabilities of the corresponding proteins.

We summarized the results and interesting observations in this area obtained by using a multi-techniques approach which provided information on metal binding abilities and on the structural features of the complexes.

Experimental techniques, together with molecular mechanics simulations were used in all the studies reported in the literature.

In particular, by using different and complementary experimental methods such as UV–vis, CD, XAS, XANES, EXAFS and NMR spectroscopies, together with potentiometric titration methods, different but complementary information has been obtained.

While potentiometric studies were fundamental to obtain information on the speciation of the different nickel complexes depending on the metal to ligand molar ratios as well as on the pH values used in the studied systems.

The spectroscopic approach was, instead, fundamental in order to have information on the chromophore involved in the binding, the geometry of the coordination sites as well as, following metal binding, on the conformational changes of the fragments.

In particular, from NMR techniques it was possible to gain information at the atomic level about the structure and dynamics of the metal peptide fragments in solution.

The thermodynamic and structural properties of the nickel complexes of peptides [43] and in particular those containing histidyl and cysteinyl residues have been recently reviewed [91–93].

The following topics have been considered:

i the stoichiometry of the nickel species, as number of metal ions bound per peptide unit;
ii the donor atoms involved in the binding and the coordination environment of nickel ion;
iii the conformational changes of the fragments upon nickel binding;
iv the implication of side-chains of aminoacid residues near to the coordination site in the stabilization of the complexes;
v the evaluation of metal binding affinity through the thermodynamic stability constants calculation;
vi the comparison of nickel coordination ability to small *vs* bigger fragments as well as entire histone proteins.

Regarding the oxidative chemistry of Ni(II), this ion as a non complexed species is not able to activate mild oxidative agents, like H_2O_2 [94–96]. As a matter of fact, only low spin, diamagnetic Ni(II) complexes, mainly in a square planar geometry, can be oxidized in water to Ni(III) species [70]. These complexes can catalyze oxidative activity against DNA and proteins *via* Fenton-Weiss like mechanisms especially by the involvement of hydroxyl radical species. The participation in Fenton redox cycle, by the formation of high oxidation number of metal ions and ROS species can cause the *in vivo* damage of DNA through modifications on nucleobases, as well as single or double strands breaks, depurination or cross links. This damage is the starting point for the genotoxic effect exerted by carcinogenic metals.

The following results can be summarized from those reported in the literature, regarding the coordination behavior of Ni(II) toward all the histone fragments investigated:

- Ni(II) ion forms complexes all over the pH range with all the investigated portions;
- even at low pH value, histidine or, when present, cysteine are the anchoring sites for metal binding, giving octahedral, high spin, paramagnetic species;
- by raising the pH over 7, in all cases, Ni(II) is able to deprotonate successive peptide nitrogen atoms from the backbone until square planar, low spin, diamagnetic 4N species were formed; the driving force in the shift from the octahedral to the square planar geometry is the formation of stable five membered chelate rings;
- all fragments, as expected, undergo conformational changes to accommodate the metal ion in the binding site and the stability constants values are, usually, not very high especially with the small peptides.

In addition, when long hydrophobic side-chains, as those from lysine or arginine residues, are close to the binding sites, they can stabilize metal binding by shielding the coordination site.

Finally, the binding constants values increase by increasing the length of the fragments and, as expected, by passing from the fragments to the entire proteins, due to the hydrophobic environment present inside the molecule.

In conclusion, all the fragments can be divided into two groups: those whose nickel complexes have peculiar oxidative and hydrolytic properties, such as complexes from H3, H2A and H2B and those whose complexes formation has been correlated to changes in levels of posttranslational histone modifications [3,39,97–103], especially acetylation, such as those from histone H4, including H4 protein itself, or methylation and ubiquitylation such as those from H2B.

The evidence described above demonstrates that the binding mode and the structural properties of the coordinated nickel species may cause damage, which, either alone or in a synergic way, operate on the cell nucleus *via* direct or indirect actions. The damage includes: (i) oxidative against nucleobasis or DNA strands [104,105] and repair patterns [106,107], that are genotoxic or promutagenic effects and (ii) all the changes in global levels of post-translational histone modifications, including acetylation, methylation as well as ubiquitylation [3,108,109], that are epigenetic effects.

Both mechanisms [110–112], genotoxic which can act as the initiation and epigenetic by which promotion and progression trigger, may actively participate together [28].

All these effects, resulting from the coordination ability of Ni(II) ions, might be important in the molecular mechanism of Ni-induced carcinogenesis and provide an interesting molecular view of nickel bioinorganic chemistry [113].

Concluding, we would also like to highlight that the competition for Ni(II) ions between target histones on one side, and cellular low

molecular weight ligands on the other side [114,115], should be taken into account depending, especially, on the concentration of metal ion and the condition of its uptake. Such an issue should be considered in future research for the molecular mechanisms of cellular damage exerted by toxic metal ions.

Acknowledgments

This work was supported by Regione Autonoma Sardegna FSE Sardegna 2007-2013 L.R.7/2007 "Promozione della ricerca scientifica e dell'innovazione tecnologica in Sardegna", L.R.7/2010 and by Fondazione Banco di Sardegna.

Appendix A. Supplementary data

Supplementary data associated with this article can be found, in the online version, at http://dx.doi.org/10.1016/j.ccr.2013.02.022.

References

[1] IARC Monographs on the Evaluation of Carcinogenic Risks to Humans, Chromium, Nickel and Welding, vol. 49, IARC, Lyon, France, 1990, pp. 257–445.
[2] M. Costa, Annu. Rev. Pharmacol. Toxicol. 31 (1991) 321–337.
[3] Y.W. Lee, C.B. Klein, B. Kargacin, K. Salnikow, J. Kitahara, K. Dowjat, A. Zhitkovich, N.T. Christie, M. Costa, Mol. Cell. Biol. 15 (1995) 2547–2557.
[4] K. Salnikow, S. Cosentino, C. Klein, M. Costa, Mol. Cell. Biol. 14 (1994) 851–858.
[5] D. Alberts, D. Bray, J. Lewis, M. Raff, K. Roberts, J.D. Watson, Molecular Biology of the Cells, 3rd ed. Part II, Garland Publishing Inc., New York, 1994, pp. 335–399.
[6] Z. Nackerdien, K.S. Kasprzak, G. Rao, B. Halliwell, M. Dizdaroglu, Cancer Res. 51 (1991) 5837–5842.
[7] N. Cotelle, E. Tremolieres, J.L. Bernier, J.P. Catteau, J.P. Henichart, J. Inorg. Biochem. 46 (1992) 7–15.
[8] M. Halcrow, G. Christou, Chem. Rev. 94 (1994) 2421–2481.
[9] L.D. Pettit, J.E. Gregor, H. Kozłowski, in: R.W. Hay, J.R. Dilworth, K.B. Nolan (Eds.), Perspectives on Bioinorganic Chemistry, vol. 1, JAI Press, London, 1991, pp. 1–41.
[10] H. Sigel, R.B. Martin, Chem. Rev. 82 (1982) 385–426.
[11] C. Burks, M. Cassidy, M.J. Cinkosky, K.E. Cumella, P. Gilna, J.E.-D. Hayden, T.A. Kelley, M. Kelly, D. Kristofferson, J. Ryals, Nucleic Acids Res. 19 (Suppl.) (1991) 2221–2225.
[12] C. von Holt, W.F. Brandt, H.J. Greyling, G.G. Lindsey, J.D. Retief, J.A. Rodrigues, S. Schwager, B.T. Sewell, in: P.M. Wassarman, R.D. Kornberg (Eds.), Methods in Enzymology, vol. 170, Nucleosomes, Academic Press, San Diego, 1989, pp. 503–523.
[13] E.F. Pettersen, T.D. Goddard, C.C. Huang, G.S. Couch, D.M. Greenblatt, E.C. Meng, T.E. Ferrin, J. Comput. Chem. 25 (2004) 1605–1612.
[14] C.A. Davey, D.F. Sargent, K. Luger, A.W. Maeder, T.J. Richmond, J. Mol. Biol. 319 (2002) 1097–1113.
[15] M.A. Zoroddu, T. Kowalik-Jankowska, H. Kozłowski, H. Molinari, K. Salnikow, L. Broday, M. Costa, Biochim. Biophys. Acta 1475 (2000) 163–168.
[16] M.A. Zoroddu, M. Peana, T. Kowalik-Jankowska, H. Kozłowski, M. Costa, J. Chem. Soc. Dalton Trans. 3 (2002) 458–465.
[17] M.A. Zoroddu, L. Schinocca, T. Kowalik-Jankowska, H. Kozłowski, K. Salnikow, M. Costa, Environ. Health Perspect. 110 (Suppl. 5) (2002) 719–723.
[18] P.E. Carrington, F. Al-Mjeni, M.A. Zoroddu, M. Costa, M.J. Maroney, Environ. Health Perspect. 110 (Suppl. 5) (2002) 705–708.
[19] M.A. Zoroddu, M. Peana, S. Medici, Dalton Trans. (2007) 379–384.
[20] W. Bal, J. Lukszo, K.S. Kasprzak, Chem. Res. Toxicol. 9 (1996) 535–540.
[21] W. Bal, J. Lukszo, M. Jezowska-Bojczuk, K.S. Kasprzak, Chem. Res. Toxicol. 8 (1995) 683–692.
[22] W. Bal, V. Karantza, E.N. Moudrianakis, K.S. Kasprzak, Arch. Biochem. Biophys. 364 (1999) 161–166.
[23] B.C. Wang, J. Rose, G. Arents, E.N. Moudrianakis, J. Mol. Biol. 236 (1994) 179–188.
[24] K. Luger, A.W. Mader, R.K. Richmond, D.F. Sargent, T.J. Richmond, Nature 389 (1997) 251–260.
[25] R.D. Camerini-Otero, G. Felsenfeld, Proc. Natl. Acad. Sci. U.S.A. 74 (1977) 5519–5523.
[26] T. Karavelas, G. Malandrinos, N. Hadjiliadis, P. Mlynarz, H. Kozłowski, M. Barsan, I. Butler, Dalton Trans. (2008) 1215–1223.
[27] W. Bal, J. Lukszo, K. Bialkowski, K.S. Kasprzak, Chem. Res. Toxicol. 11 (1998) 1014–1023.
[28] W. Bal, R. Liang, J. Lukszo, S.H. Lee, M. Dizdaroglu, K.S. Kasprzak, Chem. Res. Toxicol. 13 (2000) 616–624.
[29] M. Mylonas, J.C. Plakatouras, N. Hadjiliadis, W. Bal, J. Chem. Soc. Dalton Trans. 22 (2002) 4296–4306.
[30] A.A. Karaczyn, W. Bal, S.L. North, R.M. Bare, V.M. Hoang, R.J. Fisher, K.S. Kasprzak, Chem. Res. Toxicol. 16 (2003) 1555–1559.
[31] M. Mylonas, J.C. Plakatouras, N. Hadjiliadis, Dalton Trans. (2004) 4152–4160.
[32] M. Mylonas, J.C. Plakatouras, N. Hadjiliadis, K.D. Papavasileiou, V.S. Melissas, J. Inorg. Biochem. 99 (2005) 637–643.
[33] A. Krezel, M. Mylonas, E. Kopera, W. Bal, Acta Biochim. Pol. 53 (2006) 721–727.
[34] A.A. Karaczyn, R.Y. Cheng, G.S. Buzard, J. Hartley, D. Esposito, K.S. Kasprzak, Ann. Clin. Lab. Sci. 39 (2009) 251–262.
[35] A.M. Nunes, K. Zavitsanos, G. Malandrinos, N. Hadjiliadis, Dalton Trans. 39 (2010) 4369–4381.
[36] A.M. Nunes, K. Zavitsanos, R. Del Conte, G. Malandrinos, N. Hadjiliadis, Dalton Trans. (2009) 1904–1913.
[37] A.M. Nunes, K. Zavitsanos, R. Del Conte, G. Malandrinos, N. Hadjiliadis, Inorg. Chem. 49 (2010) 5658–5668.
[38] T. Karavelas, M. Mylonas, G. Malandrinos, J.C. Plakatouras, N. Hadjiliadis, P. Mlynarz, H. Kozłowski, J. Inorg. Biochem. 99 (2005) 606–615.
[39] L. Broday, W. Peng, M.H. Kuo, K. Salnikow, M. Zoroddu, M. Costa, Cancer Res. 60 (2000) 238–241.
[40] L.D. Pettit, S. Pyburn, W. Bal, H. Kozłowski, M. Bataille, J. Chem. Soc. Dalton Trans. (1990) 3565–3570.
[41] G.F. Bryce, R.W. Roeske, F.R. Gurd, J. Biol. Chem. 240 (1965) 3837–3846.
[42] P. Młynarz, N. Gaggelli, J. Panek, M. Stasiak, G. Valensin, T. Kowalik-Jankowska, M.T. Leplawy, Z. Latajka, H. Kozłowski, J. Chem. Soc. Dalton Trans. (2000) 1033–1038.
[43] H. Kozłowski, W. Bal, M. Dyba, T. Kowalik-Jankowska, Coord. Chem. Rev. 184 (1999) 319–346.
[44] W. Bal, H. Kozłowski, G. Kupryszewski, Z. Mackiewicz, L. Pettit, R. Robbins, J. Inorg. Biochem. 52 (1993) 79–87.
[45] R.W. Woody, in: V. Hruby (Ed.), The Peptides, vol. 7, Academic Press, New York, 1985, pp. 15–114.
[46] D.F. Shullenberg, P. Eason, E.C. Long, J. Am. Chem. Soc. 115 (1993) 11038–11039.
[47] Q. Liang, P.D. Eason, E.C. Long, J. Am. Chem. Soc. 117 (1995) 9625–9631.
[48] W. Bal, G.N. Chmurny, B.D. Hilton, P.J. Sadler, A. Tucker, J. Am. Chem. Soc. 118 (1996) 4727–4728.
[49] M.M. Yamashita, L. Wesson, G. Eisenman, D. Eisenberg, Proc. Natl. Acad. Sci. U.S.A. 87 (1990) 5648–5652.
[50] L. Regan, Annu. Rev. Biophys. Biomol. Struct. 22 (1993) 257–287.
[51] R.N. Dutnall, S.T. Tafrov, R. Sternglanz, V. Ramakrishnan, Cell 94 (1998) 427–438.
[52] D.J. Owen, P. Ornaghi, J.C. Yang, N. Lowe, P.R. Evans, P. Ballario, D. Neuhaus, P. Filetici, A.A. Travers, EMBO J. 19 (2000) 6141–6149.
[53] M. Shogren-Knaak, H. Ishii, J.M. Sun, M.J. Pazin, J.R. Davie, C.L. Peterson, Science 311 (2006) 844–847.
[54] M.A. Zoroddu, M. Peana, S. Medici, L. Casella, E. Monzani, M. Costa, Dalton Trans. 39 (2010) 787–793.
[55] B.D. Strahl, C.D. Allis, Nature 403 (2000) 41–45.
[56] X. Wang, S.C. Moore, M. Laszckzak, J. Ausio, J. Biol. Chem. 275 (2000) 35013–35020.
[57] M. Froimowitz, Biotechniques 14 (1993) 1010–1013.
[58] M.A. Zoroddu, T. Kowalik-Jankowska, H. Kozłowski, K. Salnikow, M. Costa, J. Inorg. Biochem. 84 (2001) 47–54.
[59] J.R. Daban, C.R. Cantor, Methods Enzymol. 170 (1989) 192–214.
[60] W. Bal, H. Kozłowski, R. Robbins, L.D. Pettit, Inorg. Chim. Acta 231 (1995) 7–12.
[61] W. Bal, M. Jezowska-Bojczuk, H. Kozłowski, L. Chruscinski, G. Kupryszewski, B. Witczuk, J. Inorg. Biochem. 57 (1995) 235–247.
[62] G. Hilmes, C.-Y. Yeh, F.S. Richardson, J. Phys. Chem. 80 (1976) 1798–1803.
[63] B. Lenarcik, M. Wisniewski, Pol. J. Chem. 57 (1983) 735–742.
[64] H. Kozlowski, Inorg. Chim. Acta 31 (1978) 135–140.
[65] P.G. Daniele, E. Prenesti, G. Ostacoli, J. Inorg. Biochem. 61 (1996) 165–177.
[66] J.M. Tsangaris, J.W. Chang, R.B. Martin, Arch. Biochem. Biophys. 130 (1969) 53–58.
[67] H. Kozlowski, A. Lebkiri, C.O. Onindo, L.D. Pettit, J.F. Galey, Polyhedron 14 (1995) 211–218.
[68] K. Panagiotou, M. Panagopoulou, T. Karavelas, V. Dokorou, A. Hagarman, J. Soffer, R. Schweitzer-Stenner, G. Malandrinos, N. Hadjiliadis, Bioinorg. Chem. Appl. (2008) 257038.
[69] K. Zavitsanos, A.M. Nunes, G. Malandrinos, C. Kallay, I. Sovago, V. Magafa, P. Cordopatis, N. Hadjiliadis, Dalton Trans. (2008) 6179–6187.
[70] C.I. Coyle, E.I. Stiefel, in: J.R. Lancaster (Ed.), The Bioinorganic Chemistry of Nickel, VCH, New York, 1988, pp. 1–28.
[71] M. Anke, B. Groppel, H. Kronemann, M. Grun, IARC Sci. Publ. (1984) 339–365.
[72] E. Denkhaus, K. Salnikow, Crit. Rev. Oncol. Hematol. 42 (2002) 35–56.
[73] K. Salnikow, A. Zhitkovich, Chem. Res. Toxicol. 21 (2008) 28–44.
[74] R. Doll, L.G. Morgan, F.E. Speizer, Br. J. Cancer 24 (1970) 623–632.
[75] G.A. Kerckaert, R.A. LeBoeuf, R.J. Isfort, Fundam. Appl. Toxicol. 34 (1996) 67–72.
[76] C.F. Kuper, R.A. Woutersen, P.J. Slootweg, V.J. Feron, Mutat. Res. 380 (1997) 19–26.
[77] A.C. Miller, S. Mog, L. McKinney, L. Luo, J. Allen, J. Xu, N. Page, Carcinogenesis 22 (2001) 115–125.
[78] G.G. Fletcher, F.E. Rossetto, J.D. Turnbull, E. Nieboer, Environ. Health Perspect. 102 (Suppl. 3) (1994) 69–79.
[79] N.W. Biggart, M. Costa, Mutat. Res. 175 (1986) 209–215.
[80] F.Z. Arrouijal, H.F. Hildebrand, H. Vophi, D. Marzin, Mutagenesis 5 (1990) 583–589.
[81] B. Kargacin, C.B. Klein, M. Costa, Mutat. Res. 300 (1993) 63–72.

[82] P. Sen, M. Costa, Cancer Res. 45 (1985) 2320–2325.
[83] M. Costa, M.P. Abbracchio, J. Simmons-Hansen, Toxicol. Appl. Pharmacol. 60 (1981) 313–323.
[84] M.P. Abbracchio, J. Simmons-Hansen, M. Costa, J. Toxicol. Environ. Health 9 (1982) 663–676.
[85] M.P. Abbracchio, J.D. Heck, M. Costa, Carcinogenesis 3 (1982) 175–180.
[86] R.M. Evans, P.J. Davies, M. Costa, Cancer Res. 42 (1982) 2729–2735.
[87] M. Costa, J.D. Heck, Adv. Inorg. Biochem. 6 (1984) 285–309.
[88] T. Davidson, H. Chen, M.D. Garrick, G. D'Angelo, M. Costa, Mol. Cell. Biochem. 279 (2005) 157–162.
[89] W. Bal, J. Lukszo, K.S. Kasprazak, Chem. Res. Toxicol. 9 (1996) 535–540.
[90] K.S. Kasprzak, W. Bal, A.A. Karaczyn, J. Environ. Monit. 5 (2003) 183–187.
[91] T. Kowalik-Jankowska, H. Kozłowski, E. Farkas, I. Sovago, in: A. Sigel, H. Sigel, R.K.O. Sigel (Eds.), Metal Ions in Life Sciences, vol. 2, Wiley & Sons, Chichester, UK, 2007, pp. 63–108.
[92] K. Kulon, D. Valensin, W. Kamysz, R. Nadolny, E. Gaggelli, G. Valensin, H. Kozlowski, Dalton Trans. (2008) 5323–5330.
[93] D. Witkowska, M. Rowińska-Żyrek, G. Valensin, H. Kozłowski, Coord. Chem. Rev. 256 (2012) 133–148.
[94] J.E. Lee, R.B. Ciccarelli, K.W. Jennette, Biochemistry 21 (1982) 771–778.
[95] K.S. Kasprzak, M.P. Waalkes, L.A. Poirier, Toxicol. Appl. Pharmacol. 82 (1986) 336–343.
[96] L.K. Tkeshelashvili, T.M. Reid, T.J. McBride, L.A. Loeb, Cancer Res. 53 (1993) 4172–4174.
[97] A.A. Karaczyn, F. Golebiowski, K.S. Kasprzak, Chem. Res. Toxicol. 18 (2005) 1934–1942.
[98] A. Karaczyn, S. Ivanov, M. Reynolds, A. Zhitkovich, K.S. Kasprzak, K. Salnikow, J. Cell. Biochem. 97 (2006) 1025–1035.
[99] H. Chen, Q. Ke, T. Kluz, Y. Yan, M. Costa, Mol. Cell. Biol. 26 (2006) 3728–3737.
[100] Q. Ke, T. Davidson, H. Chen, T. Kluz, M. Costa, Carcinogenesis 27 (2006) 1481–1488.
[101] F. Golebiowski, K.S. Kasprzak, Mol. Cell. Biochem. 279 (2005) 133–139.
[102] C.B. Klein, M. Costa, Mutat. Res. 386 (1997) 163–180.
[103] C.B. Klein, K. Conway, X.W. Wang, R.K. Bhamra, X.H. Lin, M.D. Cohen, L. Annab, J.C. Barrett, M. Costa, Science 251 (1991) 796–799.
[104] K.S. Kasprzak, Cancer Invest. 13 (1995) 411–430.
[105] K.S. Kasprzak, in: N. Hadjiliadis (Ed.), Cytotoxic, Mutagenic and Carcinogenic Potential of Heavy Metals Related to Human Environment, NATO ASI Series 2, Environment, vol. 26, Kluwer, Dordrecht, 1997, pp. 73–92.
[106] H. Dally, A. Hartwig, Carcinogenesis 18 (1997) 1021–1026.
[107] M. Hartmann, A. Hartwig, Carcinogenesis 19 (1998) 617–621.
[108] Y. Yan, T. Kluz, P. Zhang, H.B. Chen, M. Costa, Toxicol. Appl. Pharmacol. 190 (2003) 272–277.
[109] M. Nakao, Gene 278 (2001) 25–31.
[110] A. Arita, M. Costa, Metallomics 1 (2009) 222–228.
[111] Y. Chervona, A. Arita, M. Costa, Metallomics 4 (2012) 619–627.
[112] W. Bal, K.S. Kasprzak, Toxicol. Lett. 127 (2002) 55–62.
[113] W. Kaim, B. Schwederski, Bioinorganic Chemistry: Inorganic Elements in the Chemistry Life. An Introduction and Guide, Wiley, Chichester, 1994, p. 172.
[114] S. Lynn, F.H. Yew, J.-W. Hwang, M.-J. Tseng, K.Y. Jan, Carcinogenesis 15 (1994) 2811–2816.
[115] K. Salnikow, M. Gao, V. Voitkun, X. Huang, M. Costa, Cancer Res. 54 (1994) 6407–6412.
[116] E. Kopera, A. Krezel, A.M. Protas, A. Belczyk, A. Bonna, A. Belczyk, A. Bonna, A. Wyslouch-Cieszynska, J. Poznanski, W. Bal, Inorg. Chem. 49 (2010) 6636–6645.
[117] E. Kopera, A. Belczyk-Ciesielska, W. Bal, PLoS ONE 7 (5) (2012) e36350.